Metal to insulator transition at the surface of V_2O_3 thin films: an *in-situ* view

M. Caputo,[1,2] J. Jandke,[1] E. Cappelli,[3] S. Kumar Chaluvadi,[4] E. Bonini Guedes,[1] M. Naamneh,[1] G. Vinai,[4] J. Fujii,[4] P. Torelli,[4] I. Vobornik,[4] A. Goldoni,[2] P. Orgiani,[4,5] F. Baumberger,[3] M. Radovic,[1] and G. Panaccione[4]

[1]*Swiss Light Source, Paul Scherrer Institut, CH-5232 Villigen, Switzerland*
[2]*Elettra Sincrotrone Trieste, s.s. 14 km 163.5 in Area Science Park, 34149 Trieste, Italy*
[3]*Department of Quantum Matter Physics, University of Geneva,*
24 Quai Ernest-Ansermet, 1211 Geneva 4, Switzerland
[4]*Istituto Officina dei Materiali (IOM)-CNR, Laboratorio TASC,*
Area Science Park, S.S. 14 km 163.5, Trieste I-34149, Italy
[5]*CNR-SPIN, UOS Salerno, Fisciano, SA, I-84084, Italy*
(Dated: July 8, 2023)

V_2O_3 has long been studied as a prototypical strongly correlated material. The difficulty in obtaining clean, well ordered surfaces, however, hindered the use of surface sensitive techniques to study its electronic structure. Here we show by mean of X-ray diffraction and electrical transport that thin films prepared by pulsed laser deposition can reproduce the functionality of bulk V_2O_3. The same films, when transferred *in-situ* , show an excellent surface quality as indicated by scanning tunnelling microscopy and low energy electron diffraction, representing a viable approach to study the metal-insulator transition (MIT) in V_2O_3 by means of angle-resolved photoemission spectroscopy. Combined, these two aspects pave the way for the use of V_2O_3 thin films in device-oriented heterostructures.

I. INTRODUCTION

Since decades V_2O_3 and Cr-doped V_2O_3 are studied as prototypical systems for studying a pure Mott-Hubbard transition [1]. The temperature-doping phase diagram of V_2O_3 is presented in figure 1: undoped V_2O_3 shows a paramagnetic (PM) - antiferromagnetic insulator (AFI) electronic phase transition, accompanied with a corundum - monoclinic structural phase transition at temperatures around 150 K. This temperature can be lowered using Ti doping, down to the point where it vanishes for doping levels greater than 5%. On the contrary, Cr doping brings the occurrence of a paramagnetic insulator (PI) phase, that shares the same corundum structure of the parent compound.

The trigonally distorted octahedral crystal field of vanadium sesquioxide splits the t_{2g} states into a doubly degenerate e_g^π and a nondegenerate a_{1g} states, to be filled by the two valence electrons of V^{3+} atoms [2]. Initial low spin - single band models used to describe the electronic structure of V_2O_3 had to be abandoned when a polarisation-dependent X-ray Absorption Spectroscopy (XAS) study showed that both e_g^π and a_{1g} states are populated in all the three phases, albeit with different occupation ratio among them [3, 4]. In the meanwhile, dynamical mean-field theory (DMFT) studies approached the multi-orbital problem, unraveling a strong many-body enhancement of the trigonal crystal field splitting that brings the e_g^π states almost entirely below the Fermi level, leaving the Fermi surface of the PM phase to be composed predominantly by a_{1g} states [5]. However, recent theoretical studies based on full charge consistency reduced this strongly polarised scenario [6, 7].

Until recently, no Angle resolved photoemission spectroscopy (ARPES) studies were available to guide DMFT calculations. The first ARPES data presented by Lo Vec-
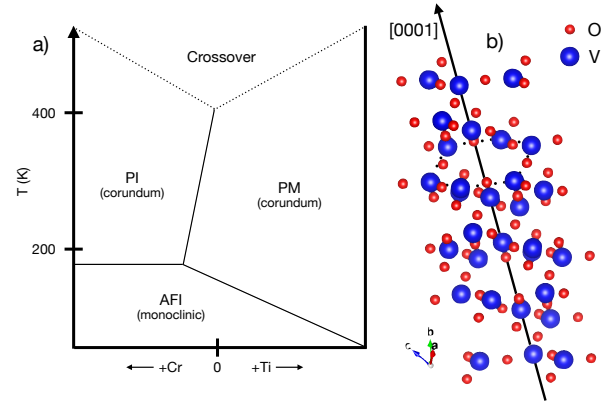

FIG. 1. (a) The temperature-doping phase diagram of V_2O_3(b) V_2O_3 crystal structure in its high-temperature corundum phase: in blue (red) the V (O) atoms. The arrow indicates the [0001] direction, whose surface is the one investigated here, while the black dotted line is a guide for the eye to underline the honeycomb lattice surface perpendicular to the [0001] direction.

chio et al. [8], however, challenged the current narrative around the electronic structure of the PM phase, showing the presence of both electron and hole pockets, that is a clear signature of a considerable weight of e_g^π states at the Fermi level. The authors were able to obtain a highly ordered (0001) surface of V_2O_3 by annealing a polished single crystal in oxygen rich atmosphere (oxygen-annealing). However, controlling this preparation step is not trivial, and slight variations in oxygen pressure or annealing temperature will result in surfaces being far different from the truncated V_2O_3 bulk [9], like vanadyl-

terminated, oxygen or vanadium rich terminations [10], or, in some cases, with vanadium in a completely different oxidation state [11].

Using alternative approaches, however, it is possible to obtain surfaces that can be a good approximation of a bulk truncation. Fabrication of thin films using pulsed laser deposition (PLD) avoids any of the steps traditionally used in surface preparation (such as high-energy ion sputtering or annealing in vacuum or oxygen-rich atmosphere) that might lead to surfaces that are not representative of the bulk. This approach has been used in the past, for instance, to control the surface termination and correct doping of $YB_2C_3O_7$ [12], making possible to visualise the expected ortho-II band folding otherwise not visible in cleaved single crystals. Moreover, using thin films adds yet new possibilities to manipulate material properties, like the emergence of thermodynamically unfavored phases [13], dimensionality control [14, 15], substrate induced strain [16], and hetero-structuring [17, 18]. Finally, the use of thin films ensures a higher degree of control in the MIT occurrence, mitigating the known fragility that bulk V_2O_3 crystals, like other materials showing structural transitions, exhibit upon repeated transition cycles.

Besides studies of fundamental interest, V_2O_3 thin films can be one of the building blocks of useful heterostructures for the emerging field of Mottronics [19], where a precise control of bulk functionalities, as well as surface and interface properties, are mandatory for the fabrication of reliable devices. Critical aspects in oxide functional heterostructure for device applications are stoichiometry (which defines the bulk functionalities), and surface/interface terminations (in order to modify the bulk functionality with the other blocks of the heterostructure).

In order to actually use V_2O_3 thin films as a reliable platform for fundamental studies, but also as a starting point for device-oriented heterostructures, finding a growth protocol that results in a functional V_2O_3 bulk, and that shows at the same time a surface representative of the bulk properties and functionalities, is mandatory. Here we show that this goal can be achieved with thin films prepared by PLD. X-ray diffraction and transport measurements indicate a bulk-like growth, with a clear MIT occurring around 185 K. Surface quality has been verified by X-ray photoemission spectroscopy (XPS), XAS, scanning tunnelling microscopy (STM) and low energy electron diffraction (LEED), showing long range order and correct V_2O_3 surface electronic structure. Moreover, comparing *in-situ* and *ex-situ* transferred sample, spectroscopy indicates a clear surface degradation, stressing the importance for all the surface studies of an *in-situ* transfer protocol. Finally, ARPES could capture the band reorganisation occurring at the MIT at the very topmost layers of V_2O_3.

II. METHODS

Samples were grown starting from commercially available V_2O_3 targets (SurfaceNet GmBH and Stanford Advanced Materials) ablated using the fundamental harmonic of a Nd:YAG laser (1064 nm) onto (0001)-oriented sapphire (Al_2O_3) substrates [20]. Depositions were performed in vacuum ($p < 10^{-7}$ mbar), with the substrate kept at a temperature of 750°C.

Electrical characterisation was carried out by standard four probes dc technique in the van-der-Pauw configuration, with a bias pulsed and reversed current of 1mA. Scanning tunnelling microscopy (STM) experiment was performed with an atomic-resolution UHV apparatus, immediately after the growth of the samples. STM topographic maps were acquired in a constant-current mode by using a tungsten tip.

XPS measurements were performed at the APE-HE beamline at the Elettra Synchrotron, using a Scienta R3000 hemispherical electron energy analyzer, with the sample at 45° with respect to the impinging linearly polarized light and the analyser normal to the surface. The energy resolution for both XAS and XPS was set to 100 meV. XAS measurements were taken in total electron yield (TEY) mode, normalizing the intensity of the sample current to the incident photon flux current at each energy value. ARPES measurements were performed at the HighRes endstation of the SIS beamline at the SLS, using a Scienta R4000 electron alayser. In this case, the total energy resolution was better than 20 meV.

Both systems host a PLD setup connected *in-situ* to the experimental chambers where synchrotron-radiation-based measurements are performed.

III. RESULTS AND DISCUSSION

A. Structural characterisation and transport properties

Structural characterisation of a 56 nm thick V_2O_3 films was performed by means of *ex-situ* x-ray diffraction (XRD) and x-ray reflectivity (XRR), as shown in Figure 2. XRD symmetrical $\theta - 2\theta$ scans of V_2O_3 films only contain $(0\,0\,6l)$ peaks, indicating the preferential c-axis orientation of the film along the [0001] crystallographic direction of the Al_2O_3 substrates and confirming the R-3c:H trigonal crystal structure. Structural data was compared to those reported in literature for bulk V_2O_3 [21]. In particular, V_2O_3 shows a R-3c trigonal spacegroup, with hexagonal cell lattice parameters a=4.9018 Å and c=13.9690 Å. The out-of-plane parameter was determined by the (006) Bragg diffraction peak in the symmetrical $\theta - 2\theta$ scan resulting in 13.97 ± 0.01 Å; in-plane parameter was determined by the (0 2 10) asymmetric Bragg reflection, which was expected at Q_x and Q_y values of 0.35739 and 0.55260 r.l.u., respectively; the experimental value of Q_x was found at 0.358 r.l.u., corresponding
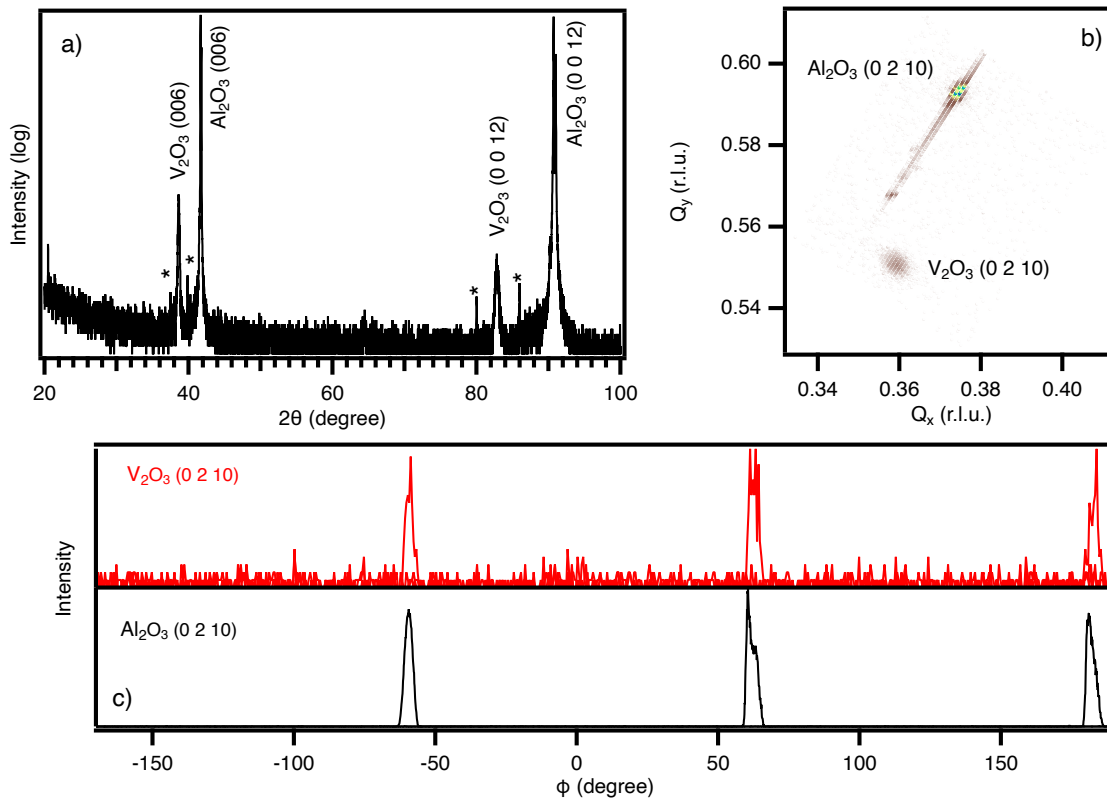
FIG. 2. (a) Symmetrical $\theta - 2\theta$ scan of a V_2O_3 film grown on an Al_2O_3 substrates. Peaks marked with a star are originated by the radiation emitted by the K_β line of the Cu anode. (b) Reciprocal space map around the $(0\,2\,10)$ asymmetric Bragg reflections of both film and substrate - Q_x and Q_y are reported in reciprocal lattice unit (r.l.u.); (c) Azimuthal ϕ-scan of both film and substrate around the $(0\,2\,10)$ asymmetric Bragg reflections.

to a=4.89 ± 0.02 Å; By considering the experimental values, the lattice parameters of our thin films fully match those reported for bulk V_2O_3, therefore confirming that films are fully relaxed. Interestingly, the azimuthal ϕ-scan of V_2O_3 only shows a three-fold symmetry, as for the Al_2O_3 substrate with no trace of twin-domain with a 60 degree in-plane rotation.

Film thickness and surface roughness were investigated by low-angle X-ray reflectivity (XRR) (simulations of the data have been performed by means of the IMD package of XOP software), as shown in Figure 3a. Oscillation simulated for a film roughness of 1 nm (red curve) are clearly damped for $\theta - 2\theta$ values greater than 4 degrees, while still visible on the experimental data (black curve), setting an upper limit for surface roughness. In order to give a better estimation for the mean surface roughness we performed *in-situ* STM. Figure 3b shows a 150x150 nm image representative of the whole sample. Large terraces of the order of tens of nanometers are visible, with steps height of 0.6 or 1.2 nm (panel c, line profile along the line in panel b). The overall root mean square (RMS) height variation calculated over the same image is about 0.8 nm, indicating a very low surface roughness of the grown samples, consistent with the XRR data.

Excellent surface quality is also confirmed by atomic resolution STM (figure 4a), and its corresponding two dimensional Fourier transform (2D-FT), showing perfect hexagonal symmetry. The long-range order of the surface was also probed by *in-situ* LEED. Figure 4b reports the LEED patterns obtained using primary electron with kinetic energy of 105 eV and 135 eV respectively. The pattern shows sharp diffraction spots arranged with a hexagonal symmetry, without any surface reconstruction, and without circular rings connecting them, indicating no trace of randomly oriented domains. By changing the primary energy it is possible to vary the intensity ratio between the two subsets of threefold-symmetric spots, indicating a threefold symmetry for the three-dimensional crystal and a growth with predominantly one domain orientation.

Finally, transport properties of V_2O_3 (Figure 5) show the hysteretical behaviour of resistivity as a function of temperature expected for its MIT. It is worth noting that the thermal hysteresis of the electronic transport properties might not be as pronounced as in single crystals (where it is several orders of magnitude) because of the structural disorder characteristic of thin films. In particular, as also observed in other oxide systems [22], struc-
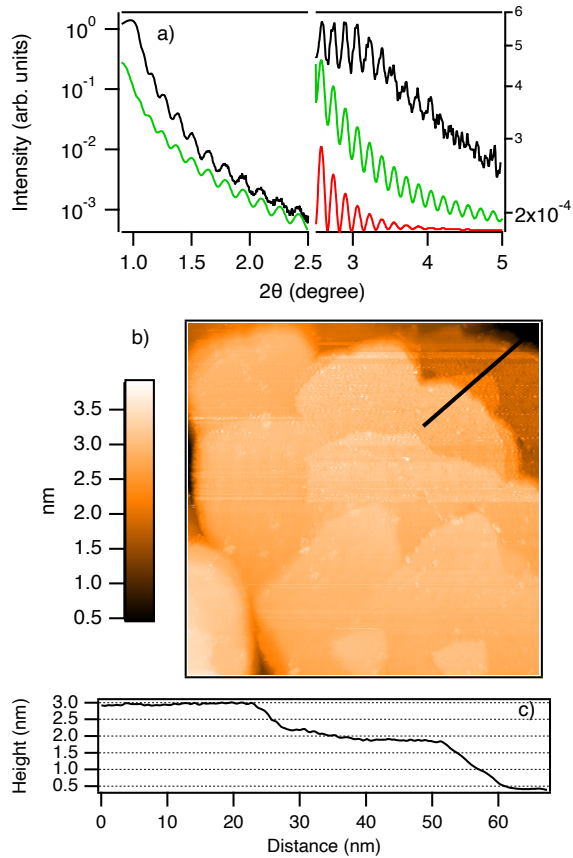
FIG. 3. (a) XRR curve of a V_2O_3 film grown on (0001)-Al_2O_3 substrate: the black curve is the experimental data, compared to a simulated signal from an atomically perfect surface (green curve) and a simulated 1-nm rough surface (red curve). (b) Surface topography seen by STM, with a profile line (panel c) taken along the black line.

tural disorder and inhomogeneities - characteristic of thin films - promote phase-separated domains, each of them characterised by a first-order MIT with slightly different transition temperatures. This last can result into a *broader* transition in resistivity measurements.

B. Core level spectroscopy characterisation

XAS and XPS experiments were performed on both *in-situ* and *ex-situ* transferred V_2O_3 samples. *In-situ*-transferred samples were moved under UHV conditions (base pressure $< 2 \cdot 10^{-10}$ mbar) to the end station of the APE-HE beamline, directly after the growth process.

XAS spectra of the V $L_{2,3}$ absorption edges of *in-situ* transferred and *ex-situ* V_2O_3 films are shown in figure 6a. Comparing the two, a substantial degradation of the V_2O_3 films upon exposure to air is recognisable. The *in-situ* transferred sample (red curve) shows the same features measured on the reference *in-situ* cleaved single crystal sample (red dashed line, from [23]), in particular
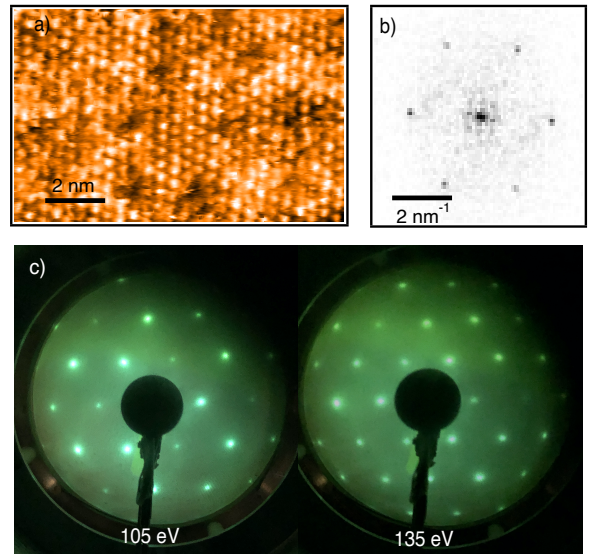

FIG. 4. (a) Atomic resolution STM image, with its 2D-FT (b). (c) LEED patterns of a V_2O_3 film acquired using electrons of 105 eV and 135 eV kinetic energy.
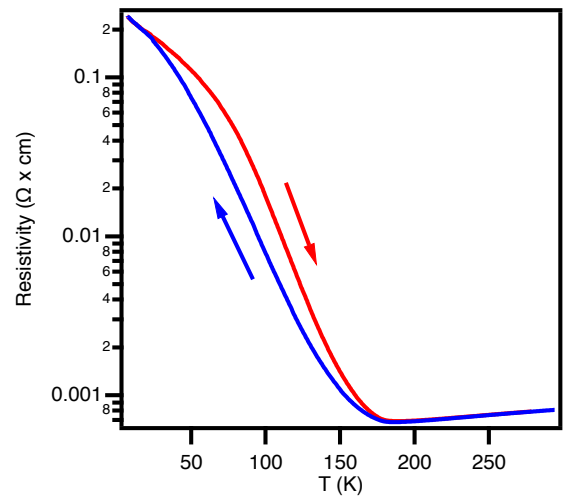

FIG. 5. Resistivity behaviour as a function of the temperature of a V_2O_3 thin film measured during a cooling (blue) / warming (red) cycle.

a sharp L_3 edge at 517.7 eV, anticipated by a shoulder peak at 515 eV and a small pre-edge contribution at 514 eV, followed by a significant extra peak in the valley region between L_3 and L_2 peaks, with the latter presenting a quite marked double-peak feature. All these detailed features are expected from both theoretical calculations [3, 24] and from previously reported experimental results on *in-situ* cleaved single crystals [23–25] and thin films [26]. On the other hand, the *ex-situ* sample (black curve) presents much broader features, with a wider L_3 edge and no double peak on the L_2 edge: a clear sign of surface degradation. The shift of the peaks and the marked change in shape of the L_2 edge could be tentatively at-
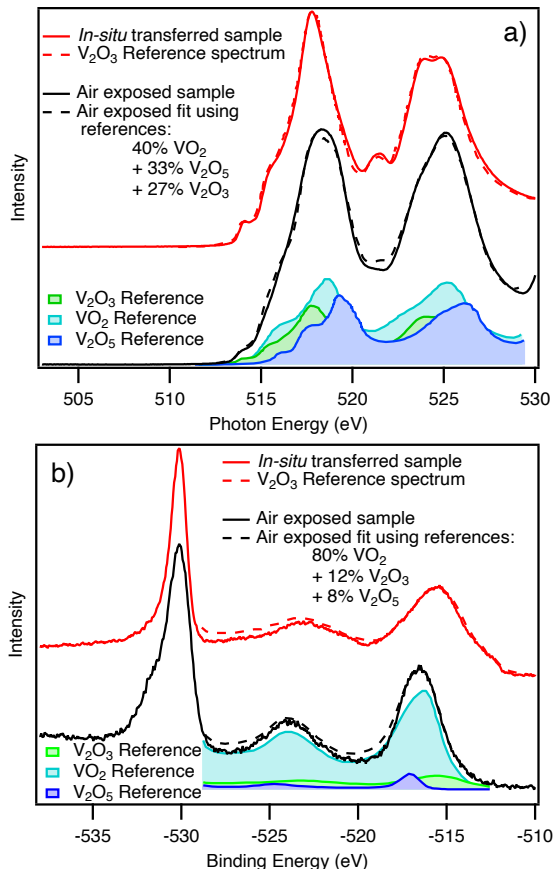
FIG. 6. a) XAS spectra at V $L_{2,3}$ absorption edges of *in-situ* (red) and *ex-situ* (black) transferred V_2O_3 thick films; they are compared with reference spectra of V_2O_3 VO_2, and V_2O_5 form [23]. b) V 2p and O 1s XPS peaks for the same V_2O_3 samples measured with a photon energy of 900 eV and compared with cleaved single crystals reference spectra; references from [23].

tributed to a contribution coming from the formation of VO_2 and/or V_2O_5 [24] upon air exposure, or to a significative change in the electronic configuration of the topmost layers induced by molecular adsorption. In order to investigate in detail this aspect, the XAS spectrum of the air exposed sample is compared with a linear combination of reference spectra acquired on V_2O_3 VO_2, and V_2O_5 single crystals (black dashed line, references from [23]). From this comparison, it is evident that just a small fraction (roughly one third) of the total XAS intensity can be attributed to V_2O_3 while the predominant contribution arises from vanadium in a different oxidation state (4+ for VO_2, and 5+ for V_2O_5).

Similarly, significant differences arise when comparing the V 2p XPS spectra of the *in-situ* and *ex-situ* V_2O_3 (figure 6b - $h\nu$=900 eV). In particular, the *ex-situ* sample does not show the shake-down shoulder at 512.5 eV binding energy. This feature is a fingerprint of the metallic state of V_2O_3, being interpreted as a more efficient

core-hole screening [27], and its absence indicate the absence of metallicity of the topmost layers. In this case the fraction of signal originated from V_2O_3 is even lower than the one observed by XAS. This observation could be attributed to the higher surface sensitivity of photoemission with respect to XAS acquired in TEY mode. The distinct fractions of V_2O_3 identified by XAS and XPS is thus consistent with a scenario in which the healthy V_2O_3 bulk is buried under layers of crystal degraded by the air exposure.

It is also worth noticing that the O1s core level (centred at 530 eV of binding energy) is strongly affected by exposure to air: a new shoulder at higher binding energy appears, most likely due to the appeearence of hydroxyl/vanadyl groups at the surface [9].

C. ARPES investigation

Lastly, we turn our attention to the possibility of studying the MIT using ARPES on the *in-situ* -transferred samples. For this purpose we grew a V_2O_3 film and transferred it *in-situ* in the high resolution end station of the SIS beamline at the Swiss Light Source.

Figure 7b shows a cut in the k_x - k_y plane of the Fermi surface (in the following, for semplicity, just FS) of the V_2O_3 film acquired at a temperature of 190K with a photon energy of 58 eV. This choice of photon energy allows to cut the three dimensional Brillouin zone (BZ) roughly half way between Γ and Z (see figure 7a: red dashed lines indicate the cuts in the BZ corresponding to the two photon energies used in this study, and calculated using an inner potential value of 14 eV as in ref [8]). Probing this region of the reciprocal space permits an easier comparison with the one already published in [8] (acquired on polished and oxygen-annealed single crystal). The shape of the FS resembles the one measured in ref [8], with arclike structures that leave an hollow in the BZ center. The most striking difference between the two is the symmetry of this structure: threefold in the case of ref [8], while sixfold in our case. Most likely this difference arises from the presence of two 60 degrees rotated domains in the film, resulting in an apparent sixfold symmetry instead of the intrinsic threefold one. The two sets of dashed lines (green and blue) highlight the contribution coming from the two rotated domains, while the green continuous line marks the edge of the first Biroullin zone for the green-oriented domain.

In Figure 7c we report the (symmetrised) E_B vs k cut along the dashed line shown in panel b, but acquired with a photon energy close to the bulk Γ point (82 eV), in which a faint parabolic-shaped feature emerges from the incoherent background. A momentum-distribution curve (MDC) integrated across the Fermi level among the red dashed lines (reported in panel e, red dots) can be fitted using two Lorentzian functions (red continuous line) $I = \frac{1}{\pi} \frac{\Gamma}{(x-x_0)^2+\Gamma^2}$, with the Fermi momentuim $k_F = x_0$ and the electron mean free path $\lambda = \frac{1}{\Gamma}$. The Fermi
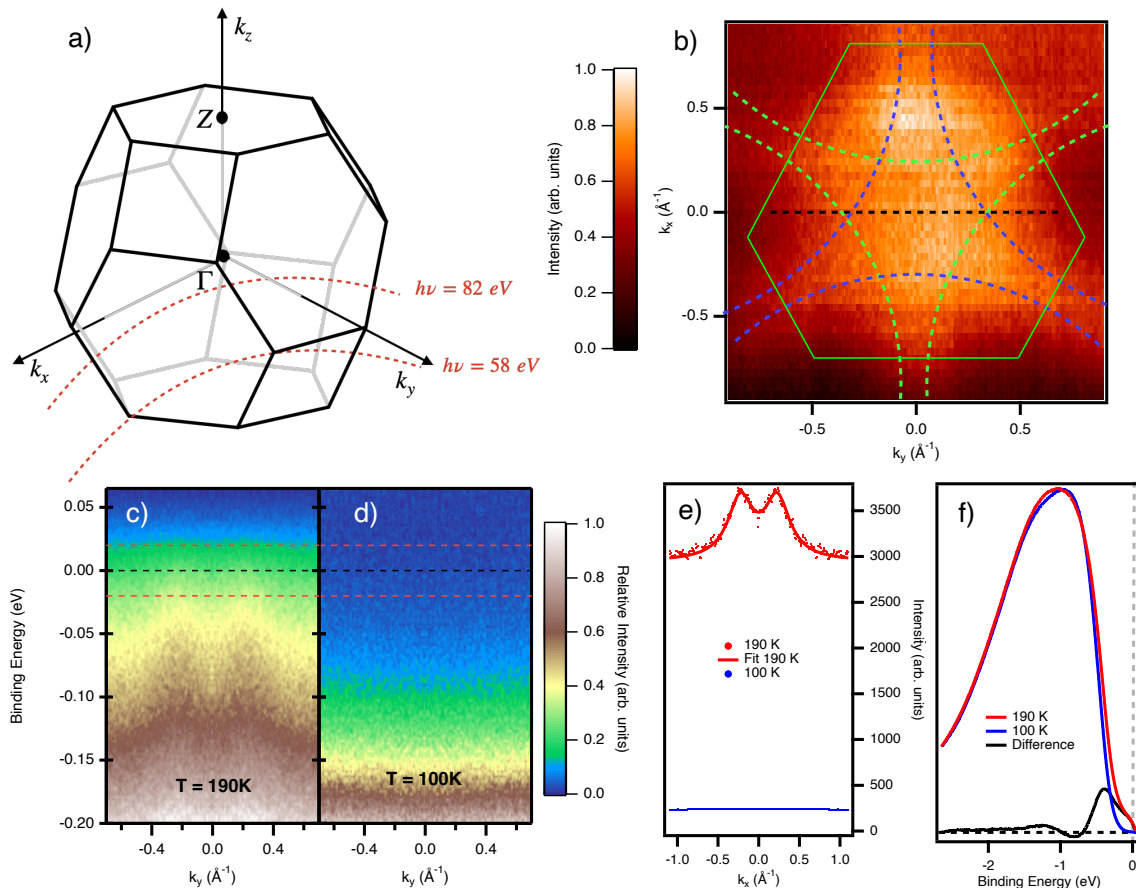
FIG. 7. Panel a: Brillouin Zone of V_2O_3 with indicated the k_x, k_y, and k_z notation used in the following. Red dashed lines indicates the cuts in the k_z dimension at the used photon energy. Panel b: Fermi surface acquired at a photon energy of 58 eV at 190 K. The black dashed line represents the position where the cuts shown in panels c and d are taken, while the blue and green dashed lines are guide to the eyes to mark the arc-like structures described in the text. Panels c and d: E_B vs k cuts acquired with a photon energy of 82 eV at 190 K and 100 K respectively. The black dashed lines mark the position of the Fermi level, while the red dashed lines denote the energy interval used to create the MDCs reported in panel e. Panel e: comparison between MDCs at low and high temperature. Panel f: comparison between the momenta integrated spectra in a wider range above (red) and below (blue) the MIT temperature, together with their difference spectrum (black).

momentum extracted from our fit is $k_F = \pm 0.23\,\text{Å}^{-1}$, in fair accordance with those find in ref [8]. The energy distribution-curve (EDC) integrated over all the momenta (panel f, red) shows a clear Fermi cut.

Upon cooling down the sample to 100K, the parabolic feature, as well as the incoherent spectral weight present at the Fermi level, vanishes, as clearly visible from Figure 7d, and its EDC and MDC reported in panels e and f. The comparison between the MDCs at low and high temperature, reported in Figure 7e, shows a clear suppression of spectral weight at the Fermi level. Finally, the angle-integrated spectra at high (red) and low (blue) temperature are reported in figure 7f, together with their difference spectrum (black). The latter shows a spectral weight redistribution from lower to higher E_B in the range from -0.7 to -1.5 eV.

It is worth noticing that the whole spectral weight between the Fermi level and 0.2 eV, i.e. where the quasi-

particle lies, vanishes as a result of the metal-to-insulator transition taking place. This behaviour is similar to the one observed in nickelates, where it has been proposed that a charge disproportionation driven by temperature decrease [28] or dimensionality effect [14] results in increasing charge localisation and hence formation of a large gap in the DOS [16].

IV. CONCLUSION

Ancillary characterisation showed how our PLD-grown films grow atomically smooth, without any sign of surface reconstruction. A clear MIT could be detected using a four-probe transport system, even though the intrinsic disorder of thin films, if compared to single crystals, widens its temperature range. The use of core level spectroscopy pointed out the importance of *in-situ* transfer,

in order to preserve surface properness, fundamental in ARPES studies.

Finally, a broad dispersive band could be observed in ARPES. Upon cooling, the MIT manifested itself with the complete disappearance of this band.

More extensive ARPES investigation of these films would be highly desirable, possibly with the use of photon energies not limited in the VUV range, but also extending to the more bulk sensitive regimes of the soft and hard X-rays. This is motivated by the suggestion of different electronic correlations at bulk and surface regions of the sample [27, 29–31], which has generally been termed "surface dead layer" in many transition-metal oxides, as e.g. manganites and titanates. The use of *in-situ* transfer of samples, as in the present study, allows a better control of the surface environment, and may help to address this open question. The same holds true also for time- and space-resolved ARPES studies, that in the recent past shed new light on the MIT in pristine and doped vanadium sesquioxide [32, 33]. Moreover, the thin film

approach will also allow to explore new directions in the study of the archetypal model system V_2O_3 strain and thickness are two parameters that can easily be adjusted during the thin-film growth and that could result in a tuning of the MIT [34, 35]. Additionally, strain could be used to decouple the electronic and structural transition, allowing the study of their individual roles [36]. Proximity effects with functional layers can also induce modifications in the properties of vanadium sesquioxide, by, for instance, controlling the magnetic frustration and long range AFM ordering [37, 38], or controlling the strain by using piezoelectric substrates [39].

V.   ACKNOWLEDGMENT

[1] N. F. Mott, Metal-insulator transition, Rev. Mod. Phys. **40**, 677 (1968).

[2] S. Y. Ezhov, V. I. Anisimov, D. I. Khomskii, and G. A. Sawatzky, Orbital occupation, local spin, and exchange interactions in V_2O_3, Phys. Rev. Lett. **83**, 4136 (1999).

[3] J.-H. Park, L. H. Tjeng, A. Tanaka, J. W. Allen, C. T. Chen, P. Metcalf, J. M. Honig, F. M. F. de Groot, and G. A. Sawatzky, Spin and orbital occupation and phase transitions in V_2O_3, Phys. Rev. B **61**, 11506 (2000).

[4] R. J. O. Mossanek and M. Abbate, Importance of the $V3d - O2p$ hybridization in the mott-hubbard material V_2O_3, Phys. Rev. B **75**, 115110 (2007).

[5] A. I. Poteryaev, J. M. Tomczak, S. Biermann, A. Georges, A. I. Lichtenstein, A. N. Rubtsov, T. Saha-Dasgupta, and O. K. Andersen, Enhanced crystal-field splitting and orbital-selective coherence induced by strong correlations in V_2O_3, Phys. Rev. B **76**, 085127 (2007).

[6] D. Grieger and F. Lechermann, Effect of chromium doping on the correlated electronic structure of V_2O_3, Phys. Rev. B **90**, 115115 (2014).

[7] X. Deng, A. Sternbach, K. Haule, D. N. Basov, and G. Kotliar, Shining light on transition-metal oxides: Unveiling the hidden fermi liquid, Phys. Rev. Lett. **113**, 246404 (2014).

[8] I. Lo Vecchio, J. D. Denlinger, O. Krupin, B. J. Kim, P. A. Metcalf, S. Lupi, J. W. Allen, and A. Lanzara, Fermi surface of metallic V_2O_3 from angle-resolved photoemission: Mid-level filling of e_g^π bands, Phys. Rev. Lett. **117**, 166401 (2016).

[9] S. Surnev, M. Ramsey, and F. Netzer, Vanadium oxide surface studies, Progress in Surface Science **73**, 117 (2003).

[10] J. Schoiswohl, M. Sock, S. Surnev, M. Ramsey, F. Netzer, G. Kresse, and J. Andersen, V_2O_3 (0001) surface terminations: from oxygen- to vanadium-rich, Surface Science **555**, 101 (2004).

[11] B. Van Bilzen, P. Homm, L. Dillemans, C.-Y. Su, M. Menghini, M. Sousa, C. Marchiori, L. Zhang, J. W. Seo, and J.-P. Locquet, Production of VO_2 thin films through post-deposition annealing of V_2O_3 films, Thin Solid Films **591**, 143 (2015).

[12] Y. Sassa, M. Radović, M. Månsson, E. Razzoli, X. Y. Cui, S. Pailhès, S. Guerrero, M. Shi, P. R. Willmott, F. Miletto Granozio, J. Mesot, M. R. Norman, and L. Patthey, Ortho-II band folding in $YBa_2Cu_3O_{7-\delta}$ films revealed by angle-resolved photoemission, Phys. Rev. B **83**, 140511 (2011).

[13] S. Surnev, G. Kresse, M. G. Ramsey, and F. P. Netzer, Novel interface-mediated metastable oxide phases: Vanadium oxides on Pd(111), Phys. Rev. Lett. **87**, 086102 (2001).

[14] P. King, H. Wei, Y. F. Nie, M. Uchida, C. Adamo, S. Zhu, X. He, I. Božović, D. G. Schlom, and K. M. Shen, Atomic-scale control of competing electronic phases in ultrathin $LaNiO_3$, Nature nanotechnology **9**, 443 (2014).

[15] M. Caputo, M. Boselli, A. Filippetti, S. Lemal, D. Li, A. Chikina, C. Cancellieri, T. Schmitt, J.-M. Triscone, P. Ghosez, S. Gariglio, and V. N. Strocov, Artificial quantum confinement in $LaAlO_3/SrTiO_3$ heterostructures, Phys. Rev. Materials **4**, 035001 (2020).

[16] R. S. Dhaka, T. Das, N. C. Plumb, Z. Ristic, W. Kong, C. E. Matt, N. Xu, K. Dolui, E. Razzoli, M. Medarde, L. Patthey, M. Shi, M. Radović, and J. Mesot, Tuning the metal-insulator transition in $NdNiO_3$ heterostructures via fermi surface instability and spin fluctuations, Phys. Rev. B **92**, 035127 (2015).

[17] N. Plumb, M. Kobayashi, M. Salluzzo, E. Razzoli, C. Matt, V. Strocov, K. Zhou, M. Shi, J. Mesot, T. Schmitt, L. Patthey, and M. Radović, Evolution of the $SrTiO_3$ surface electronic state as a function of $LaAlO_3$ overlayer thickness, Applied Surface Science **412**, 271 (2017).

[18] V. Polewczyk, S. K. Chaluvadi, P. Orgiani, G. Panaccione, G. Vinai, G. Rossi, and P. Torelli, Tuning the magnetic properties of V_2O_3/CoFeB heterostructures across the V_2O_3 structural transition, Phys. Rev. Materials **5**, 034413 (2021).

[19] Y. Tokura, M. Kawasaki, and N. Nagaosa, Emergent functions of quantum materials, Nature Physics **13**, 1056 (2017).

[20] S. K. Chaluvadi, D. Mondal, C. Bigi, D. Knez, P. Rajak, R. Ciancio, J. Fujii, G. Panaccione, I. Vobornik, G. Rossi, and P. Orgiani, Pulsed laser deposition of thin films by means of Nd : YAG laser source operating at its 1st harmonic: recent approaches and advances, Journal of Physics: Materials (2021).

[21] L. W. Finger and R. M. Hazen, Crystal structure and isothermal compression of Fe_2O_3, Cr_2O_3, and V_2O_3 to 50 kbars, Journal of Applied Physics **51**, 5362 (1980).

[22] E. Dagotto, T. Hotta, and A. Moreo, Colossal magnetoresistant materials: the key role of phase separation, Physics Reports **344**, 1 (2001).

[23] R. Zimmermann, R. Claessen, F. Reinert, P. Steiner, and S. Hüfner, Strong hybridization in vanadium oxides: evidence from photoemission and absorption spectroscopy, Journal of Physics: Condensed Matter **10**, 5697 (1998).

[24] M. Abbate, H. Pen, M. Czyżyk, F. de Groot, J. Fuggle, Y. Ma, C. Chen, F. Sette, A. Fujimori, Y. Ueda, and K. Kosuge, Soft x-ray absorption spectroscopy of vanadium oxides, Journal of Electron Spectroscopy and Related Phenomena **62**, 185 (1993).

[25] O. Müller, J. P. Urbach, E. Goering, T. Weber, R. Barth, H. Schuler, M. Klemm, S. Horn, and M. L. denBoer, Spectroscopy of metallic and insulating V_2O_3, Phys. Rev. B **56**, 15056 (1997).

[26] B. Sass, C. Tusche, W. Felsch, N. Quaas, A. Weismann, and M. Wenderoth, Structural and electronic properties of epitaxial V_2O_3 thin films, Journal of Physics: Condensed Matter **16**, 77 (2003).

[27] G. Panaccione, M. Altarelli, A. Fondacaro, A. Georges, S. Huotari, P. Lacovig, A. Lichtenstein, P. Metcalf, G. Monaco, F. Offi, L. Paolasini, A. Poteryaev, O. Tjernberg, and M. Sacchi, Coherent peaks and minimal probing depth in photoemission spectroscopy of mott-hubbard systems, Phys. Rev. Lett. **97**, 116401 (2006).

[28] S. Johnston, A. Mukherjee, I. Elfimov, M. Berciu, and G. A. Sawatzky, Charge disproportionation without charge transfer in the rare-earth-element nickelates as a possible mechanism for the metal-insulator transition, Phys. Rev. Lett. **112**, 106404 (2014).

[29] G. Borghi, M. Fabrizio, and E. Tosatti, Surface dead layer for quasiparticles near a mott transition, Phys. Rev. Lett. **102**, 066806 (2009).

[30] F. Rodolakis, B. Mansart, E. Papalazarou, S. Gorovikov, P. Vilmercati, L. Petaccia, A. Goldoni, J. P. Rueff, S. Lupi, P. Metcalf, and M. Marsi, Quasiparticles at the mott transition in V_2O_3: Wave vector dependence and surface attenuation, Phys. Rev. Lett. **102**, 066805 (2009).

[31] E. Papalazarou, M. Gatti, M. Marsi, V. Brouet, F. Iori, L. Reining, E. Annese, I. Vobornik, F. Offi, A. Fondacaro, S. Huotari, P. Lacovig, O. Tjernberg, N. B. Brookes, M. Sacchi, P. Metcalf, and G. Panaccione, Valence-band electronic structure of V_2O_3: Identification of v and o bands, Phys. Rev. B **80**, 155115 (2009).

[32] G. Lantz, B. Mansart, D. Grieger, D. Boschetto, N. Nilforoushan, E. Papalazarou, N. Moisan, L. Perfetti, V. L. Jacques, D. Le Bolloc'h, *et al.*, Ultrafast evolution and transient phases of a prototype out-of-equilibrium mott–hubbard material, Nature communications **8**, 1 (2017).

[33] S. Lupi, L. Baldassarre, B. Mansart, A. Perucchi, A. Barinov, P. Dudin, E. Papalazarou, F. Rodolakis, J.-P. Rueff, J.-P. Itié, *et al.*, A microscopic view on the mott transition in chromium-doped V_2O_3, Nature communications **1**, 1 (2010).

[34] L. Dillemans, T. Smets, R. R. Lieten, M. Menghini, C.-Y. Su, and J.-P. Locquet, Evidence of the metal-insulator transition in ultrathin unstrained V_2O_3 thin films, Applied Physics Letters **104**, 071902 (2014).

[35] E. B. Thorsteinsson, S. Shayestehaminzadeh, and U. B. Arnalds, Tuning metal-insulator transitions in epitaxial V_2O_3 thin films, Applied Physics Letters **112**, 161902 (2018).

[36] S. S. Majid, D. K. Shukla, F. Rahman, K. Gautam, R. J. Choudhary, V. G. Sathe, and D. M. Phase, Stabilization of metallic phase in V_2O_3 thin film, Applied Physics Letters **110**, 173101 (2017).

[37] J. C. Leiner, H. O. Jeschke, R. Valentí, S. Zhang, A. T. Savici, J. Y. Y. Lin, M. B. Stone, M. D. Lumsden, J. Hong, O. Delaire, W. Bao, and C. L. Broholm, Frustrated magnetism in mott insulating $(V_{1-x}Cr_x)_2O_3$, Phys. Rev. X **9**, 011035 (2019).

[38] J. Trastoy, A. Camjayi, J. del Valle, Y. Kalcheim, J.-P. Crocombette, D. A. Gilbert, J. A. Borchers, J. E. Villegas, D. Ravelosona, M. J. Rozenberg, and I. K. Schuller, Magnetic field frustration of the metal-insulator transition in V_2O_3, Phys. Rev. B **101**, 245109 (2020).

[39] J. Sakai, M. Bavencoffe, B. Negulescu, P. Limelette, J. Wolfman, A. Tateyama, and H. Funakubo, Strain-induced resistance change in V_2O_3 films on piezoelectric ceramic disks, Journal of Applied Physics **125**, 115102 (2019).